STABILITY OF POISEUILLE FLOW

IN THE PRESENCE OF A LONGITUDINAL MAGNETIC FIELD

A. V. Proskurin and A. M. Sagalakov   UDC 537.84

The stability of the plane flow of an electrically conducting fluid with respect to small perturbations was studied at large Reynolds numbers in the presence of a longitudinal magnetic field. The dependence of the critical Reynolds number on the electrical conductivity is investigated. At large Reynolds numbers, a new branch of instability and a sudden change in the critical Reynolds numbers is found.
Key words: *hydrodynamic stability, electrically conducting viscous fluid, differential sweep method.*

Introduction. The stability of a plane magnetohydrodynamic Poiseuille flows of an electrically conducting fluid with respect to small perturbations in a longitudinal magnetic field has been studied for a long time [1–7] and is of interest for the development of general theory for laminar–turbulent transition of viscous fluid flows in channels and for investigation of the bifurcation of solutions of the Navier–Stokes equations. This problem is a classical one but there are still no simple and effective methods to study Tollmien–Schlichting instability in a linear approximation at large Reynolds numbers and considerable magnetic Prandtl numbers. Experimental verification of the results and propositions of the linear theory of hydrodynamic stability is also complicated, especially at large magnetic Prandtl number.

Direct numerical simulations of instability development yield results close to experimental data [8–10]. Such calculations, however, are very complex and expensive because of the necessity of using supercomputers. In addition, it is difficult to establish the basic laws of development and stabilization of perturbations versus the parameters included in the equations, because, for each set of parameters, one has to investigate a set of perturbations of different form and amplitude. Furthermore, direct numerical simulation techniques have substantial limitations on the Reynolds number and the order of the system of equations to be solved. At the same time, the capabilities of modern computational facilities allow small perturbations of magnetohydrodynamic flows to be studied using the full linearized equations of magnetic hydrodynamics over a wide range of parameters of the equations and at large Reynolds numbers.

1. Formulation of the Problem. We write the equations of magnetic hydrodynamics in dimensionless form

$$\frac{\partial \boldsymbol{H}}{\partial t} + (\boldsymbol{V}\nabla)\boldsymbol{H} = (\boldsymbol{H}\nabla)\boldsymbol{V} + \frac{1}{\mathrm{Re}_m}\,\Delta\boldsymbol{H},$$

$$\frac{\partial \boldsymbol{V}}{\partial t} + (\boldsymbol{V}\nabla)\boldsymbol{V} = -\nabla\Big(p + \mathrm{Al}\,\frac{H^2}{2}\Big) + \mathrm{Al}\,(\boldsymbol{H}\nabla)\boldsymbol{H} + \frac{1}{\mathrm{Re}}\,\Delta\boldsymbol{V}, \qquad (1)$$

$$\mathrm{div}\,\boldsymbol{H} = 0, \qquad \mathrm{div}\,\boldsymbol{V} = 0.$$

Here $\mathrm{Al} = H_0^2/(4\pi\rho V_0^2)$ is the Alfvén number, $\mathrm{Re} = V_0 d/\nu$ is the Reynolds number, and $\mathrm{Re}_m = 4\pi V_0 d\sigma/c^2$ is the magnetic Reynolds number. As the characteristic parameters we use the channel width, the flow-averaged velocity, and the intensity of the external magnetic field. We introduce Cartesian coordinates with the x axis directed

383

along the flow direction and the y axis perpendicular to the parallel planes bounding the fluid. The z axis is perpendicular to the x and y axes. The boundary of the channel corresponds to the coordinates $y = \pm 1/2$. It is reasonable to introduce the generalized pressure $P_g = p + \text{Al} H^2/2$. Thus, the structure of the equations of magnetic hydrodynamics is such that three parameters (for example, Al, Re, and Re_m) completely determine the behavior of the system for the specified channel geometry and external magnetic field. In the calculations, instead of the magnetic Reynolds number we used the magnetic Prandtl number $\text{Pr}_m = \text{Re}_m / \text{Re} = 4\pi\sigma\nu/c^2$, which is directly proportional to the electric conductivity.

The solution of system (1) can be represented as

$$\boldsymbol{V} = \boldsymbol{U} + \boldsymbol{v}, \qquad \boldsymbol{H} = \boldsymbol{H}_0 + \boldsymbol{h}, \qquad P_g = P_0 + P, \tag{2}$$

where $\boldsymbol{U} = \{U, 0, 0\}$, $\boldsymbol{H}_0 = \{1, 0, 0\}$, P_0 is the steady-state solution of system (1); $U = (3/2)(1 - 4y^2)$ and $\boldsymbol{v}$, $\boldsymbol{h}$, and P are perturbations of the velocity, magnetic field, and generalized pressure. Substitute (2) into Eqs. (1) and assuming the perturbations to be small, we obtain the linearized system of equations

$$\frac{\partial \boldsymbol{h}}{\partial t} + (\boldsymbol{U}\nabla)\boldsymbol{h} + (\boldsymbol{v}\nabla)\boldsymbol{H}_0 = (\boldsymbol{H}_0\nabla)\boldsymbol{v} + (\boldsymbol{h}\nabla)\boldsymbol{U} + \frac{1}{\text{Re}_m}\Delta\boldsymbol{h},$$

$$\frac{\partial \boldsymbol{v}}{\partial t} + (\boldsymbol{U}\nabla)\boldsymbol{v} + (\boldsymbol{v}\nabla)\boldsymbol{U} = -\nabla P + \text{Al}\,(\boldsymbol{H}_0\nabla)\boldsymbol{h} + \text{Al}\,(\boldsymbol{h}\nabla)\boldsymbol{H}_0 + \frac{1}{\text{Re}}\Delta\boldsymbol{v}, \tag{3}$$

$$\text{div}\,\boldsymbol{h} = 0, \qquad \text{div}\,\boldsymbol{v} = 0.$$

The channel walls are considered impermeable and perfectly electrically conducting. The boundary conditions for the perturbations are given by

$$y = \pm 1/2: \qquad \boldsymbol{v} = 0, \quad \boldsymbol{h} = 0.$$

We seek solutions of the linearized system of equations of magnetic hydrodynamics (3) in the form

$$\{v_x(y), v_y(y), v_z(y), h_x(y), h_y(y), h_z(y), q(y)\}\, \text{e}^{i\alpha(x - Ct) + i\beta z}, \tag{4}$$

where v_x, v_y, v_z, h_x, h_y, and h_z are projections of the perturbation amplitudes of the velocity and magnetic field intensity onto the corresponding Cartesian axes, q is the pressure perturbation amplitude, α is the longitudinal wavenumber, β is the cross-sectional wavenumber, $C = X + iY$ is the complex phase velocity, X is the proper phase velocity, and αY is the perturbation attenuation decrement (at $Y < 0$) or the perturbation growth increment (at $Y > 0$). Substitution of (4) into (3) yields the system of differential equations

$$i\alpha(U - C)h_x = i\alpha v_x + h_y U' + (h_x'' - h_x(\alpha^2 + \beta^2))/(\text{Pr}_m\,\text{Re}); \tag{5}$$

$$i\alpha(U - C)h_y = i\alpha v_y + (h_y'' - h_y(\alpha^2 + \beta^2))/(\text{Pr}_m\,\text{Re}); \tag{6}$$

$$i\alpha(U - C)h_z = i\alpha v_z + (h_z'' - h_z(\alpha^2 + \beta^2))/(\text{Pr}_m\,\text{Re}); \tag{7}$$

$$i\alpha(U - C)v_x + v_y U' = -i\alpha q + i\alpha\,\text{Al}\,h_x + (v_x'' - v_x(\alpha^2 + \beta^2))/\text{Re}; \tag{8}$$

$$i\alpha(U - C)v_y = -q' + i\alpha\,\text{Al}\,h_y + (v_y'' - v_y(\alpha^2 + \beta^2))/\text{Re}; \tag{9}$$

$$i\alpha(U - C)v_z = -i\beta q + i\alpha\,\text{Al}\,h_z + (v_z'' - v_z(\alpha^2 + \beta^2))/\text{Re}; \tag{10}$$

$$h_y' + i\alpha h_x + i\beta h_z = 0, \qquad v_y' + i\alpha v_x + i\beta v_z = 0. \tag{11}$$

We introduce the new functions: $v = \alpha v_x + \beta v_z$ and $h = \alpha h_x + \beta h_z$. Multiplying Eq. (5) by α and Eq. (7) by β, combining the results, and performing similar operations with Eqs. (8) and (10), we obtain

$$i\alpha(U - C)h = i\alpha v + \alpha h_y U' + (h'' - k^2 h)/(\text{Pr}_m\,\text{Re}),$$

$$i\alpha(U - C)h_y = i\alpha v_y + (h_y'' - k^2 h_y)/(\text{Pr}_m\,\text{Re}); \tag{12}$$

$$i\alpha(U - C)v + \alpha v_y U' = -ik^2 q + i\alpha\,\text{Al}\,h + (v'' - k^2 v)/\text{Re}; \tag{13}$$

$$i\alpha(U - C)v_y = -q' + i\alpha\,\mathrm{Al}\,h_y + (v_y'' - k^2 v_y)/\,\mathrm{Re},$$

$$v_y' + iv = 0. \tag{14}$$

Here $k^2 = \alpha^2 + \beta^2$ is the square of the wave vector. In this case, the equation $\mathrm{div}\,\boldsymbol{h} = 0$ is written as $h_y' + ih = 0$. Using this relation in Eq. (13), the quantity h can be expressed in terms of h_y. As a result, the system of differential equations (12)–(14) becomes

$$i\alpha(U - C)h = i\alpha v + \alpha h_y U' + (h'' - k^2 h)/(\mathrm{Pr}_m\,\mathrm{Re}); \tag{15}$$

$$i\alpha(U - C)h_y = i\alpha v_y + (h_y'' - k^2 h_y)/(\mathrm{Pr}_m\,\mathrm{Re}),$$

$$i\alpha(U - C)v + \alpha v_y U' = -ik^2 q - \alpha\,\mathrm{Al}\,h_y' + (v'' - k^2 v)/\,\mathrm{Re},$$

$$i\alpha(U - C)v_y = -q' + i\alpha\,\mathrm{Al}\,h_y + (v_y'' - k^2 v_y)/\,\mathrm{Re}, \tag{16}$$

$$v_y' + iv = 0.$$

It is easy to see that the quantity h is now included only in Eq. (15), which is separated from system (15), (16). We denote

$$D = i\alpha\,\mathrm{Re}\,(U - C), \qquad \Omega = i\alpha\mathrm{Pr}_m\,\mathrm{Re}\,(U - C). \tag{17}$$

Using formulas (17), we write the system of differential equations (16) in the form

$$v_y' = -iv, \qquad h_y' = \Phi, \qquad v' = Z,$$

$$\Phi' = k^2 h_y - i\alpha\,\mathrm{Re}\,\mathrm{Pr}_m v_y + \Omega h_y,$$

$$Z' = k^2 v + \alpha\,\mathrm{Re}\,\mathrm{Al}\,\Phi + ik^2\,\mathrm{Re}\,q + \alpha U'\,\mathrm{Re}\,v_y + Dv,$$

$$q' = -\frac{D}{\mathrm{Re}}v_y + i\alpha\,\mathrm{Al}\,h_y - \frac{i}{\mathrm{Re}}Z - \frac{k^2}{\mathrm{Re}}v_y.$$

This system is conveniently represented in matrix form

$$\boldsymbol{W}' = M_1\boldsymbol{W} + M_2\boldsymbol{V}, \qquad \boldsymbol{V}' = M_3\boldsymbol{W} + M_4\boldsymbol{V}, \tag{18}$$

where

$$\boldsymbol{W} = \{v, v_y, h_y\}, \qquad \boldsymbol{V} = \{\Phi, Z, q\},$$

$$M_1 = \begin{pmatrix} 0 & 0 & 0 \\ -i & 0 & 0 \\ 0 & 0 & 0 \end{pmatrix}, \qquad M_2 = \begin{pmatrix} 0 & 1 & 0 \\ 0 & 0 & 0 \\ 1 & 0 & 0 \end{pmatrix},$$

$$M_3 = \begin{pmatrix} 0 & -i\alpha\,\mathrm{Re}\,\mathrm{Pr}_m & k^2 + \Omega \\ k^2 + D & \alpha U'\,\mathrm{Re} & 0 \\ 0 & -(k^2 + D)/\,\mathrm{Re} & i\alpha\,\mathrm{Al} \end{pmatrix}, \qquad M_4 = \begin{pmatrix} 0 & 0 & 0 \\ \alpha\,\mathrm{Re}\,\mathrm{Al} & 0 & ik^2\,\mathrm{Re} \\ 0 & -i/\,\mathrm{Re} & 0 \end{pmatrix}.$$

System (15), (16) admits the Squire transformations [11]

$$k\,\mathrm{Re}_{\mathrm{eff}} = \alpha\,\mathrm{Re}, \qquad \alpha q_{\mathrm{eff}} = kq, \tag{19}$$

where $\mathrm{Re}_{\mathrm{eff}}$ is the effective Reynolds number that corresponds to the solution of the two-dimensional problem. Equation (19) leads to the relation

$$\mathrm{Re}_* = (\mathrm{Re}_{\mathrm{eff}})_*/\cos\theta, \tag{20}$$

where $\cos\theta = \alpha/k$; the quantities denoted by an asterisk are the critical values of the parameters. Consequently, two-dimensional perturbations are the most dangerous in the sense that the critical Reynolds numbers for them are smaller than the critical Reynolds numbers for three-dimensional perturbations. Nevertheless, in this case, the

Squire theorem is generally speaking inappropriate. Below, we shown how the instability regions of three-dimensional perturbations "cover" the stability regions formed by two-dimensional perturbations.

2. Numerical Method. As is known, hydrodynamic stability problems, as well as, generally, eigenvalue problems for non-self-adjoint operators can effectively be solved only numerically. In this case, standard numerical methods are usually unsuitable: the eigenfunctions of linear stability problems for viscous electrically conducting fluid flows possess "bad" properties due to the presence of small parameters $1/\mathrm{Re}$ and $1/\mathrm{Re}_m$ at the higher-order derivative in the equations. The fundamental system of solutions of such equations contains rapidly growing oscillating solutions of the form $\exp\left(\int \sqrt{i\alpha\,\mathrm{Re}\,(U-C)}\,dy\right)$, which, due to rounding errors, considerably complicates the direct numerical finding of the remaining linearly independent eigenfunctions and the solution of the eigenvalue problem.

In the numerical solution of the Orr–Sommerfield problem using the collocation method [12], the above-mentioned difficulties are eliminated due to a high quality of the approximate representation of the solution. However, as the parameter $\alpha\,\mathrm{Re}$ is increased, it is necessary to use an increasing number of expansion terms, which leads to an increase in the size of the matrix used in the collocation method and deterioration of its conditionality. At present, the collocation method is used to study the stability of simple plane flows (see, for example, [13]) at relatively small Reynolds numbers.

Effective solution of hydrodynamic stability problems is provided by step-by-step integration methods, such as the Godunov orthogonalization method, the elimination method, the differential sweep method [11, 14–16]. However, the orthogonalization and elimination procedures require a large volume of calculations, which increases rapidly with increasing order of the system solved. The differential sweep method was developed to solve hydrodynamic stability problems [11, 14]. Advantages of this method are relative simplicity, universality, and high efficiency. In addition, this method gives results of high reliability, which is confirmed, in particular, by a comparison with data obtained by other methods, including the collocation method.

The differential sweep method reduces the eigenvalue problem to a sequence of Cauchy problems for a nonlinear system of ordinary differential equations, which is easily integrated numerically. Eigenvalues are determined by direct sweep. Once an eigenvalue is determined, the corresponding eigenfunction can be found by return sweep.

In the differential sweep method, the subsurface of solutions is described by the equations

$$\boldsymbol{W} = A(y)\boldsymbol{V}, \tag{21}$$

where A is a 3×3 matrix.

Expression (21) is usually called the sweep scheme. During calculations, the sweep scheme can be changed to achieve the most favorable behavior of the coefficients of the matrix A for optimization of calculations [11].

The boundary of the channel are subjected to the conditions $\boldsymbol{W} = 0$, which lead to the boundary condition $A = 0$. In the calculations, system (18) is integrated directly at small distances from the channel boundaries with subsequent use of a particular sweep scheme.

Numerical experiments have shown that the scheme (21) defined by the boundary conditions $\boldsymbol{W} = 0$ and $A = 0$ is not optimal for integration in the middle part of the channel. From the viewpoint of computation time and simplicity of the algorithm, the most economical sweep version was the following: at small distances from the channel boundaries, sweep was conducted under the scheme (21) defined by the boundary conditions, and in the middle part of the channel, we used the reversed sweep scheme

$$\boldsymbol{V} = G\boldsymbol{W}; \tag{22}$$

in the joining of the solutions, the condition $G = A^{-1}$ is satisfied by virtue of the continuity of the eigenfunctions and their derivatives. Systems of differential equations for the matrices A and G can be obtained by differentiating Eqs. (21) and (22) and substituting expressions (18) into them. As a result, we have

$$A' = M_1 A + M_2 - A(M_3 A + M_4), \qquad G' = M_4 G + M_3 - G(M_2 G + M_1). \tag{23}$$

Equation (23) was integrated numerically from the channel boundaries to a certain middle point at which, as well as at the points of inversion of the sweep scheme, the vectors $\boldsymbol{V}$ and $\boldsymbol{W}$ should be continuous, which allows us to write the following system of algebraic equations for $\boldsymbol{W}$:

$$(G^+ - G^-)\boldsymbol{W} = 0$$

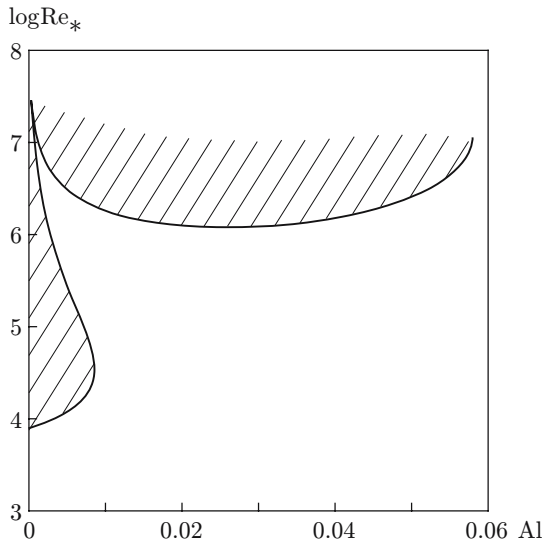Fig. 1
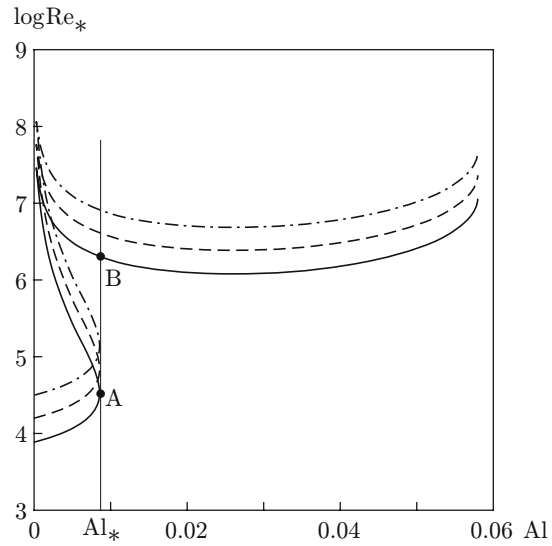
Fig. 2

Fig. 1. Curve of $Re_*(Al)$ for $Pr_m = 0.01$: the dashed region is the instability region.

Fig. 2. Curves of $Re_*(Al)$ for $Pr_m = 0.01$: the solid curve refers to $k = \alpha$; dashed curve refers to $k = 2\alpha$ [$Re_* = 2(Re_{eff})_*$], and the dot-and-dashed curve refers to $k = 4\alpha$ [$Re_* = 4(Re_{eff})_*$].

(the plus and minus signs correspond to the sweep coefficients G obtained by integration from the different boundaries of the channel). Because $\boldsymbol{W} \neq 0$, we can write the dispersion equation

$$\det (G^+ - G^-) = 0. \tag{24}$$

Numerical experiments have shown that, in this sweep scheme, the dispersion relation (24) has "good" properties. This relation was solved using iterative methods.

Once the eigenvalues are determined, $\boldsymbol{W}$ and $\boldsymbol{V}$ can be found over the entire integration interval using the return sweep.

3. Calculation Results. we consider perturbations with $k = \alpha$ (two-dimensional perturbations). Figure 1 shows a curve of the critical Reynolds number Re_* versus Alfvén number at $Pr_m = 0.01$. As $Al \to 0$, the critical Reynolds numbers tend to the values corresponding to the case of plane Poiseuille flow of a dielectric fluid. As the Alfvén number increases, the critical Reynolds number increases monotonically to $Al \approx 0.01$, after which the curve of $Re_*(Al)$ rotates toward decreasing Alfvén number, limiting the instability region from above. Above this region at Reynolds numbers of order 10^7, a new branch of instability is found, whose critical dependences are a downward convex curve.

To determine the role of two-dimensional perturbations using relation (20), we performed an analysis of three-dimensional perturbations aimed at elucidating their influence on the stability pattern. The analysis revealed regions in which three-dimensional perturbations are more dangerous than two-dimensional perturbations. Figure 2 gives a curve of the critical Reynolds number Re_* versus Alfvén number for $Pr_m = 0.01$ and $k = \alpha$, 2α, and 4α. Similar curves for other values $\cos\theta$ can be constructed using relation (20). To the lower branch of the critical dependences $k = \alpha$, we draw a vertical tangent at the point A (the corresponding Alfvén number is denoted by Al_*); at $k = \alpha$, the tangent intersects the upper branch of the critical dependences at the point B. The instability region of three-dimensional perturbations ($k > \alpha$) is on the left of the segment AB.

Thus, accounting for three-dimensional perturbations extends the instability region. At the same time, two-dimensional perturbations are the most dangerous because the critical Reynolds numbers for them are smaller than the critical Reynolds numbers for three-dimensional perturbations. The instability regions for three-dimensional perturbations can be obtained by a simple shift of the curves of $Re_*(Al)$ for two-dimensional perturbations. Next, we consider only two-dimensional perturbations, which considerably simplifies the stability analysis. To analyze the flow stability for $Al < Al_*$, it is sufficient to consider only two-dimensional perturbations.

387

Fig. 3

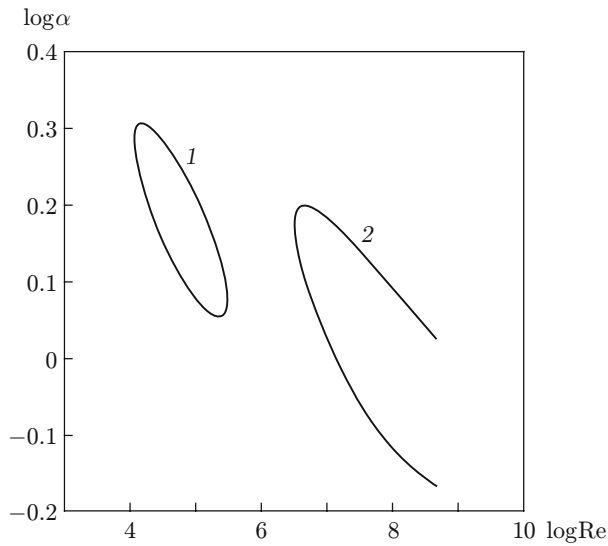

Fig. 4
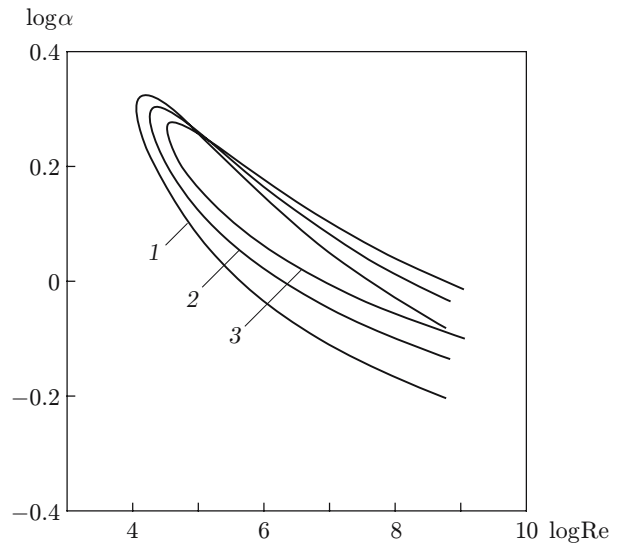
Fig. 3. Neutral curves for $\mathrm{Pr}_m = 0.01$ and $\mathrm{Al} = 0.005$: curves 1 and 2 refer to the lower and upper instability regions in Fig. 1, respectively.

Fig. 4. Neutral curves for $\mathrm{Pr}_m = 1.5$ and $\mathrm{Al} = 0.005$ (1), 0.010 (2), and 0.015 (3).

Figure 3 gives neutral curves for $\mathrm{Pr}_m = 0.01$ and $\mathrm{Al} = 0.005$. The closed neutral curve corresponds to the lower instability region in Fig. 1, and the unclosed curve to the upper instability region. The "tips" of the neutral dependences considered are on the curve of $\mathrm{Re}_*(\mathrm{Al})$ in Fig. 1. As the Alfvén number increases, the closed region of instability decreases, ultimately becoming a point. A new finding in this work is the detection of the second branch of instability at large Reynolds numbers.

Figure 4 gives neutral curves for $\mathrm{Pr}_m = 1.5$ and $\mathrm{Al} = 0.005$, 0.010, and 0.015. These curves are not closed, in contrast to the curves considered above. With increasing Alfvén number, the critical Reynolds numbers increase and the instability region is shifted somewhat toward the region of short-wave perturbations.

Figure 5a and b shows a curve of $\mathrm{Re}_*(\mathrm{Pr}_m)$ for $\mathrm{Al} = 0.010$ and 0.015, respectively. The instability regions shown in Fig. 5 have a complex shape, which is not characteristic of hydrodynamic stability problems. For $\mathrm{Pr}_m \to 0$, the values of the critical Reynolds number tend to the corresponding values for dielectric fluids, and for $\mathrm{Pr}_m > 10$, the curves of $\mathrm{Re}_*(\mathrm{Pr}_m)$ enter horizontal asymptotes which correspond to $\mathrm{Pr}_m \to \infty$. An increase in the magnetic Prandtl number from 10^{-4} to 10^{-3} leads to an insignificant increase in the critical Reynolds number. With a further increase in the magnetic Prandtl number, the curve of $\mathrm{Re}_*(\mathrm{Pr}_m)$ rotates toward decreasing magnetic Prandtl number, thus bounding the examined instability region from above. With increasing Alfvén number, this instability region becomes narrower, with the upper boundary affected by the Alfvén number the most significantly (Fig. 5). Above the examined instability region there is a stability region, which is bounded from above by the second branch of the curve of $\mathrm{Re}_*(\mathrm{Pr}_m)$. As the magnetic Prandtl number increases, the critical Reynolds numbers of this branch decrease. This arrangement of the curves of $\mathrm{Re}_*(\mathrm{Pr}_m)$ causes a sudden increase in the critical Reynolds numbers with increasing value of Pr_m. Similar behavior of the curve of $\mathrm{Re}_*(\mathrm{Pr}_m)$ is observed for $\mathrm{Pr}_m \approx 1$. In Fig. 5a, the curve of $\mathrm{Pr}_m \approx 1$ has a characteristic maximum for $\mathrm{Re}_*(\mathrm{Pr}_m)$. With a further increase in the Alfvén number, it is replaced by a narrow stability region of the given flow (Fig. 5b). **Conclusions.** The following conclusions can be drawn. An increase in the Alfvén number for some values of the parameters can lead to a sudden increase in the critical Reynolds numbers. This flow has regions of stability with respect to small two-dimensional perturbations for $\mathrm{Re} = 10^6$–10^7. Dissipation was shown to have a considerable effect on the stability of this flow. A change in the magnetic Prandtl number leads to a considerable change in the critical Reynolds numbers; a sudden stabilization of this flow can be observed. A change in the parameters (the Alfvén number and the magnetic Prandtl number) can lead to a change
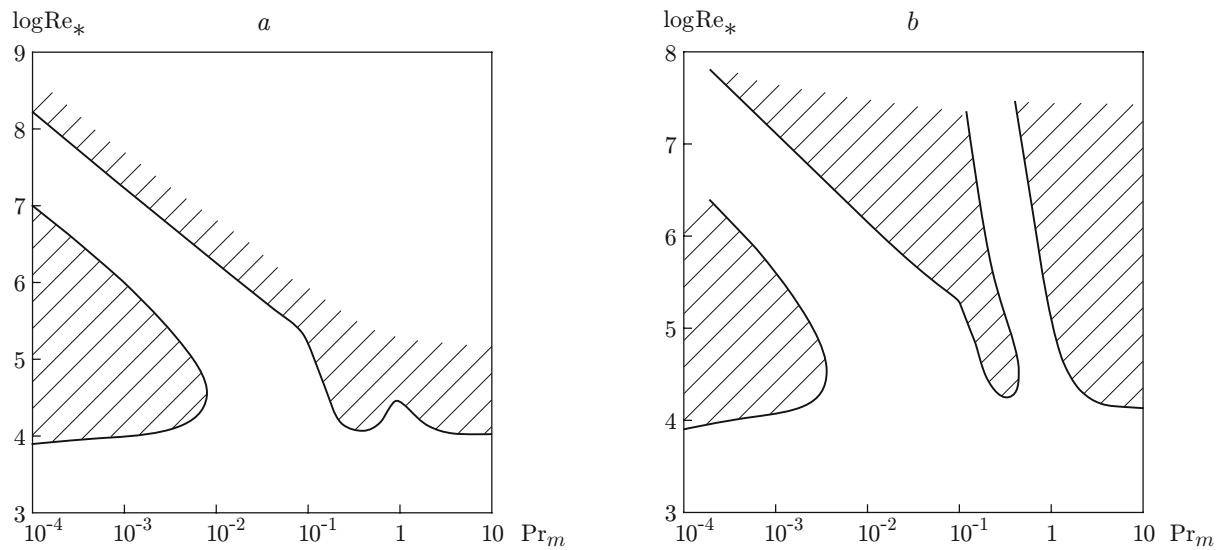
Fig. 5. Curves of $\mathrm{Re}_*(\mathrm{Pr}_m)$ for $\mathrm{Al} = 0.010$ (a) and 0.015 (b); the dashed regions are instability regions.

in the nature of the neutral curves of two-dimensional perturbations — the closed instability region is separated from the "tip" of the neutral curve, which decreases with increasing Alfvén number and then disappears. For this flow, the Squire transformations are valid but the Squire theorem is, generally speaking, inapplicable. Regions were found in which two-dimensional perturbations attenuate and three-dimensional perturbations are unstable.

In the presence of a longitudinal magnetic field, an electrically conducting fluid in a plane channel exhibits a complex and peculiar flow stability pattern. The detailed analysis of the dependence of the critical Reynolds number on the magnetic Prandtl number revealed a new branch of instability at large Reynolds numbers. This instability branch was studied in detail for $\mathrm{Re} = 10^6$–10^7 using modern computational facilities and the differential sweep method.

REFERENCES

1. D. N. Michael, "Stability of plane parallel flows of electrically conducting fluids," in: *Proc. Cambridge Philos. Soc.*, **41**, No. 1, 166–168 (1953).
2. T. Tatsumi, "MHD-stability and turbulence," *Progr. Theoret. Phys. Suppl.*, **24**, 156–193 (1962).
3. R. Betchov and W. Criminale, *Stability of Parallel Flows*, Academic Press, New York (1967).
4. J. C. R. Hunt, "On the stability of parallel flows with parallel magnetic fields," *Proc. Roy. Soc. London, Ser. A*, **293**, No. 1434, 342–358 (1966).
5. J. T. Stuart, "On the stability of viscous flow between parallel planes in the presence of a complanar magnetic field," *Proc. Roy. Soc. London, Ser. A*, **221**, 189–206 (1954).
6. E. P. Velikhov, "Stability of plane Poiseuille flow of a perfectly conducting fluid in a longitudinal magnetic field," *Zh. Éksp. Teor. Fiz.*, **36**, No. 4, 1192–1202 (1959).
7. Ko Sung Hwan, "On the stability of plane Poiseuille flow with a finite conductivity in a aligned magnetic field," *J. Fluid Mech.*, **33**, No. 3, 433–444 (1968).
8. A. Thess and O. Zikanov, "Direct numerical simulation of forced MHD turbulence at low magnetic Reynolds number," *J. Fluid Mech.*, No. 358, 299–333 (1998).
9. P. Moresko and T. Alboussierre, "Experimental study of the instability of the Hartmann layer," *J. Fluid Mech.*, No. 504, 167–181 (1998).
10. O. Zikanov, "On the instability of pipe Poiseulle flow," *Phys. Fluids*, No. 8, 2923–2932 (1996).
11. M. A. Gol'dhstik and V. N. Shtern, *Hydrodynamic Stability and Turbulence* [in Russian], Nauka, Novosibirsk (1977).
12. K. I. Babenko, Fundamentals of Numerical Analysis [in Russian], Nauka, Moscow (1986).

13. D. S. Henningson and P. J. Schmid, *Stability and Transition in Shear Flows*, Springer-Verlag, New York (2001).
14. V. A. Sapozhnikov, "Numerical solution of hydrodynamic stability problems," Author's Abstract, Cand. Dissertation in Phys.-Math. Sci., Novosibirsk (1970).
15. A. Davey, "An automatic orthonormalization method for solving stiff boundary value problem," *J. Comput. Phys.*, No. 51, 343–356 (1983).
16. A. A. Abramov, "Transfer of boundary conditions for systems of ordinary differential equations (a version of the sweep method)," *Zh. Vychisl. Mat. Mat. Fiz.*, **1**, No. 3, 542–545 (1961).